SIMULATION-DRIVEN CALIBRATION OF MHD SENSORS CONSIDERING VARIATIONS IN REYNOLDS NUMBER, TEMPERATURE, AND MAGNETIC FIELD STRENGTH

Faiza Sohail[1], Muhammad Nadeem[1], Muhammad Uzair[1], Syed Mujtaba Ul Hassan[2], Adnan Hamid[1]

[1]*Department of Chemical Engineering*
Pakistan Institute of Engineering and Applied Sciences
Islamabad, 45650, Pakistan, adnan@pieas.edu.pk (A.H.); faizasohail204@gmail.com (F.S.); mnadeem@pieas.edu.pk (M.N.); uzairhassan434@gmail.com (M.U.).
[2]*Department of Metallurgy and Materials Engineering*
Pakistan Institute of Engineering and Applied Sciences
Islamabad, 45650, Pakistan, mujtaba@pieas.edu.pk (S.H.)

Received 02 January 2024
Accepted 07 December 2024
DOI: 10.59957/jctm.v60.i2.2025.18

ABSTRACT

Liquid metal flow measurement is a challenging task in nuclear and metallurgical industries, due to the high-temperature corrosive environment. Magneto-hydrodynamic (MHD) flow meters are a good choice for such applications, due to their inherent safety, less pressure drop, bi-directional, and accurate flow measurements. In this study, sodium metal flow measurement is investigated in a circular pipe at different temperatures (T) and Reynolds number (Re), using the computational fluid dynamics tool (ANSYS Fluent®) with the MHD module, to benchmark the calibration for flow meters. Simulations are performed for T = 150 to 450°C up to Re 400, for various magnetic field strengths (B) (i.e., 0.05 to 0.4 T). It is noted that the M-shaped velocity profile develops at B ≥ 0.2 T and the maximum velocity decreases with increasing T, at a given Re and B, and it increases with increasing Re, at a given T and B. Moreover, a systematic parametric study for Re, T, and B is performed in which it is found that the voltage and Lorentz force, increases with increasing Re and decreases with increasing T, at a given B. Our results suggest that the optimum window of operation for the magnetic sensor is at T ≤ 300 and Re ≥ 200 for better performance.

Keywords: magnetic flow meters, magneto-hydrodynamics, computational fluid dynamics, liquid sodium flow, Lorentz force.

INTRODUCTION

The magnetic field affects several natural and artificial flows, generally used in industries for heating, pumping, stirring, levitating fluids, etc. [1 - 3]. The study of magnetic fields and their influence on electrically conductive fluids, either natural or man-made, is of vital importance and is classified as magneto-hydrodynamics (MHD) [4, 5]. Two main attributes must be present in such fluids; fluid must be electrically conductive and non-magnetic. These conditions limit us to fluids like liquid metals, plasmas, hot ionized gases, strong electrolytes, saltwater, etc. [6 - 8]. Among these, molten metal flows are of prime importance due to their widespread use for energy conversion, radiation shielding, and cooling in the nuclear industry and solar power stations [9, 10].

MHD flow sensors are the most suitable choice due to their inherent safety and reliability. Their non-invasiveness, penetration-less construction, low-pressure loss, good rangeability, and fast response time make them an obvious choice in above mentioned industries. Moreover, the study of electromagnetic flowmeters has also been performed, but with a limited scope [10 - 12]. Jeong presented the idea of using a samarium cobalt (SmCo) permanent magnet flow meter in a liquid sodium metal-cooled reactor and concluded that induced voltage and flow rate are linearly dependent on each other for low flow rate regimes [13]. Rajan and Aruna tested and

calibrated the side wall flow meter (SWFM), installed in a fast breeder reactor (FBR), using simulations and experiments, and developed a relationship between sodium flowrates and voltage signals. They reported that the sensitivity of SWFM increases with a rise in the mass flow rate of sodium but decreases with a rise in sodium temperature [14]. Nashine designed and developed three different types of electromagnetic flow meters. It is reported that sensitivity increases by using a SmCo magnet, an electromagnet-based flow meter that reduces high-temperature operation constraints and a probe type of permanent magnet flow meter facilitates flow measurement in large pipes [15]. Wang presented a multi-physics numerical model for the calculation of the calibration constant of a generic Lorentz force flowmeter (LFF). They proposed that theoretically, measured LFF calibration constant dominates large-scale experimental setups if seen from an economic point of view. They also concluded that the calibration constant is a function of the Reynolds Number (Re), Hartmann number (Ha), and the flow geometry [16]. Sharma performed simulations for a three-dimensional finite element model of a permanent magnet flowmeter in COMSOL Multiphysics to evaluate the sensitivity of the flowmeter in a prototype 500 MWe sodium-cooled fast breeder reactor (FBR). They reported that 3.55 mV electric voltage is produced due to a 1 m s^{-1} flow of liquid sodium in a stainless-steel pipe, which rises by 67 % to the value of 5.95 mV when a magnetic shield is placed around the flowmeter [17]. Tarabad and Baker discussed integration methods of electromagnetic flow meters for high Magnetic Reynolds Number (Re_m) [18].

Considering the above literature, MHD is an important area of research and has a wide range of applications. Despite its importance in the industry and basic research, little is known about the magnetic flow meter and its parametric importance. Even among the available studies, a complete parametric study (especially temperature dependency) has not been reported, especially for sodium metal flows, which have been widely used in the nuclear industry. In this work, Re, magnetic field, and temperature effects have been investigated on sodium metal flow, using the commercial Computational Fluid Dynamics (CFD) tool i.e., ANSYS Fluent® along with the MHD module. The voltage and Lorentz force values are obtained under the variation of all these parameters to provide the calibration data, required for designing flow sensors.

EXPERIMENTAL

Governing equations

The governing equations of MHD flow for the system are Maxwell equations and the generalized forms of these equations are presented in Eq. (1) to (4).

$$\nabla \cdot B = 0, \quad (1)$$
$$\nabla \times E = - \partial B/\partial t, \quad (2)$$
$$\nabla \cdot D = q, \quad (3)$$
$$\nabla \times H = J + \partial J/\partial t, \quad (4)$$

where B and E represent the magnetic and electric fields, respectively. H and D are the induced fields for the magnetic and electric fields, respectively, q is the electric charge density and J is the electric/induced current density. For liquid metals flow the charge density (q) and displacement current ($\partial D/\partial t$) are negligible and can be neglected [19]. The induced fields H and D are in turn defined by Eq. (5) and (6).

$$H = (1/\mu_m)B, \quad (5)$$
$$D = \varepsilon E, \quad (6)$$

where μ_m and ε are the magnetic permeability and electric permittivity [19]. Now to calculate J we know that Ohm's law for current density and fluid velocity field (U) in a magnetic field (B) is given by Eq. (7).

$$J = \sigma (E + U \times B) \quad (7)$$

where σ is the electrical conductivity of the medium. The magnetic field (B) can be decomposed into the externally imposed field (B_o) and the induced field (b**)** due to fluid motion. Also, the electric field can be defined by Eq. (8).

$$E = -\nabla V - \partial A/\partial t, \quad (8)$$

where V and A are the electric and vector potential. For a static field $b << B_o$ so, putting the modified values of B and (8) in Eq. (7) we get Eq. (9).

$$J = \sigma (-\nabla V + (U \times B_o)), \quad (9)$$

For a conducting medium, the principle of conservation of charge is given by Eq. (10).

$$\nabla \cdot J = 0, \quad (10)$$

Therefore, the electric potential is given by Eq. (11).

$$\nabla^2 \cdot V = \nabla \cdot (U \times B_o), \quad (11)$$

and the boundary conditions for the electric potential (V) are given by Eq. (12) and Eq. (13).

$$\partial V/\partial n = \nabla \cdot (U \times B_o)_{boundary} \cdot n \quad (12)$$

$$V = V_o \quad (13)$$

The first boundary condition given by Eq. (12) is valid for an insulating boundary, while the second one given by Eq. (13) is valid for a conducting boundary for which the potential is specified at the boundary. After applying the boundary condition J can be calculated from Eq. (9). Now when J is known the MHD coupling can be achieved by introducing additional source terms in the momentum (Navier-Stokes) and energy equations [19]. For the Navier-Stokes equation, the source term is the Lorentz force (F), which is a retarding force, acting opposite to the direction of flow and is given by Eq. (14).

$$F = J \times B \quad (14)$$

After incorporating F, with the assumption of steady, laminar, and incompressible flow, the simplified Navier-Stokes equation takes the following form of Eq. (15).

$$\rho (U \cdot \nabla) U = -\nabla p + \rho\mu\nabla^2 U + (J \times B), \quad (15)$$

where p is the pressure, ρ is the fluid density, and μ is the dynamic viscosity [19]. While the continuity equation is given by Eq. (16).

$$\nabla \cdot U = 0 \quad (16)$$

Furthermore, the Lorentz force in this case is dissipative and converts the mechanical energy associated with the flow to heat, thus producing a damping effect. The direction of this force is such that it is perpendicular to both the velocity of motion and the external magnetic field when the magnetic field is applied perpendicular to the flow direction. The energy equation is given by Eq. (17).

$$\partial/\partial t(\rho e) + \nabla \cdot (U(\rho e + p)) = \nabla \cdot [k\nabla T + \tau \cdot U] + Q, \quad (17)$$

where e, T, k, and τ are the energy, temperature, thermal conductivity, and shear stress, respectively [19]. Here Q is the additional source term known as the joule heating rate and is defined by Eq. (18).

$$Q = (1/\sigma)J \cdot J \quad (18)$$

Validation

MHD model embedded in the ANSYS Fluent® is validated by reproducing the results of Altinas and Ozkol [20]. This work is related to NaK metal flow in a circular pipe, using the MHD module in ANSYS Fluent®. They studied the sodium metal flow through a pipe of 300 mm in length and 10 mm in diameter with the application of a transverse magnetic field. A uniform velocity of 0.05 m s^{-1} is provided at the inlet and the development of flow with the application of magnetic field is studied. The comparison of the results obtained with the work of Altintas and Ozkol is shown in Fig. 1 [20].

Our results are in good agreement with Altintas as shown in Fig. 1. It is well established that in a laminar flow in the pipe, the maximum velocity is double the average velocity, which is 0.1 m s^{-1} in this case and our results are close to 0.1 m s^{-1} than Altintas, showing a better accuracy.

Moreover, the effects of B on the velocity profile are also studied at different field strengths i.e., 0, 0.5, 1, and 1.25 T along the length. Since it is developing flow, so velocity profile transforms into the well-known parabolic velocity profile, towards the end of the geometry. When the magnetic field is applied, the velocity profile changes due to the application of the magnetic field inducing Lorentz force with a direction opposite to the flow. This force retards the velocity, as evident in Fig. 2.

It is evident that as the flow develops progressively in the pipe, the effect of B on the flow is reduced i.e., the difference in the velocities is reduced for fully developed flow. Since the strength of the field for this case is very low, no significant change is expected. Lorentz force is induced due to a change in velocity. If the flow is developing, the change in velocity is large, which results in a large Lorentz force as compared to the fully developed flow, having a negligible change in velocity. Furthermore, it can be noticed that the field strength decreases the center line velocity, consequently increasing the velocity near the wall, such that the momentum remains conserved.

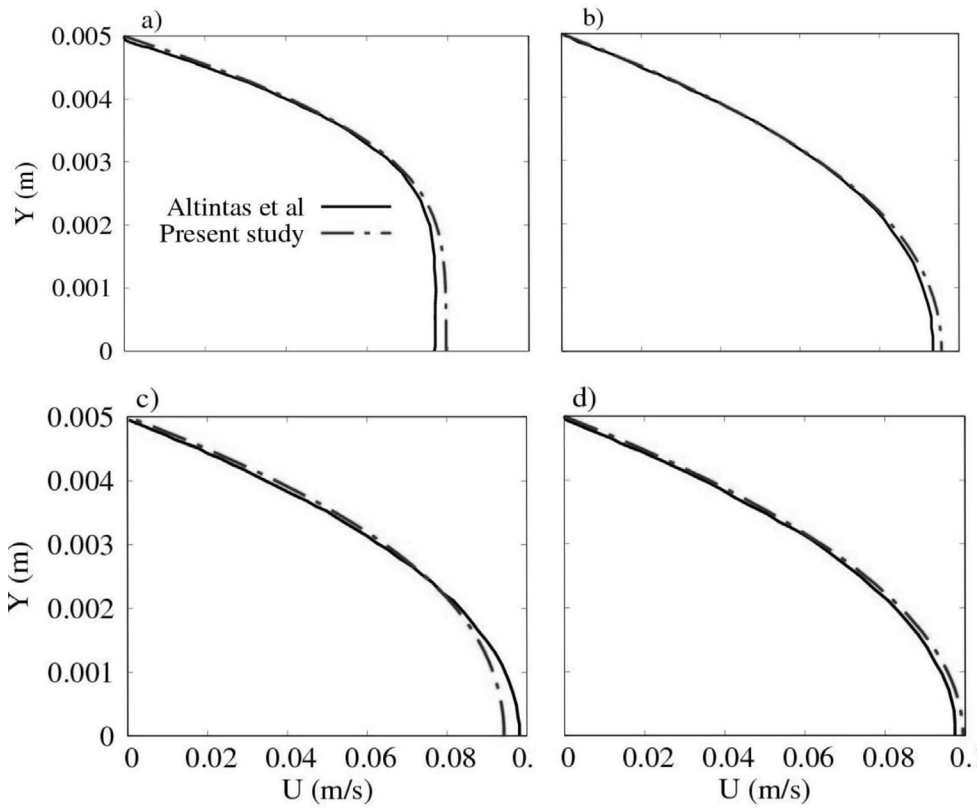

Fig. 1. Comparison of the velocity profile of the present study with Altintas and Ozkol [20] at (a) 50 mm, (b) 150 mm, (c) 250 mm, and (d) 298 mm.

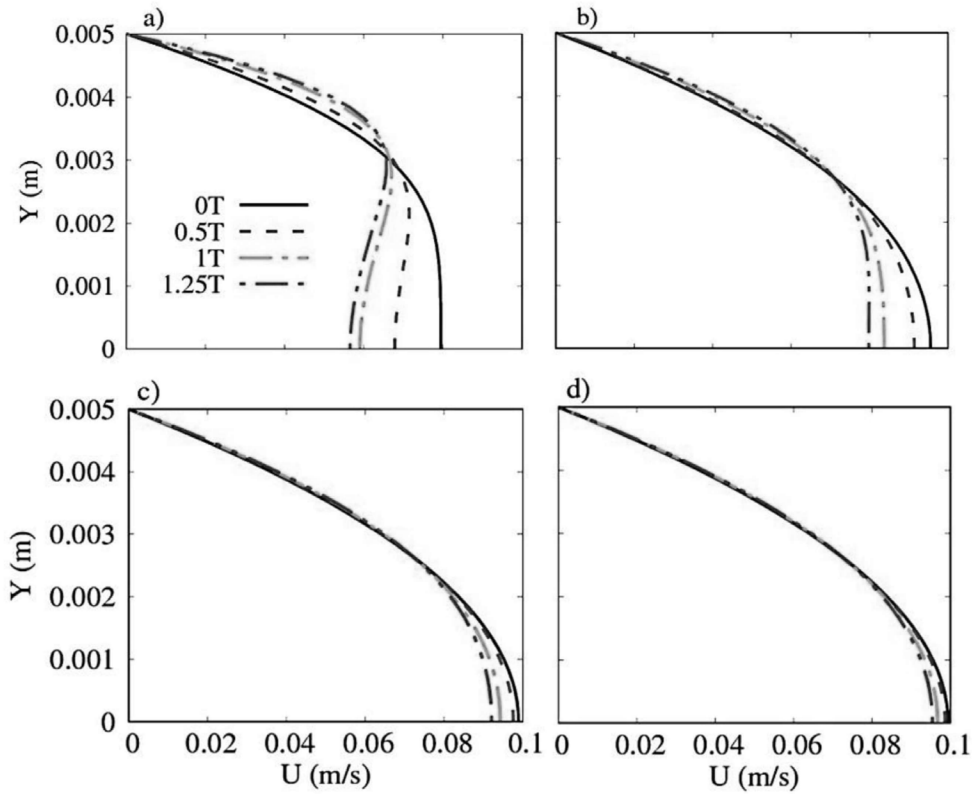

Fig. 2. Velocity profiles at different points along the length (a) 50 mm, (b) 150 mm, (c) 250 mm, and (d) 298 mm.

Problem description and mesh independence

In the present work, Sodium metal flow in a circular pipe is investigated with the application of a transverse magnetic field, as schematically depicted in Fig. 3. The steady laminar flow is maintained in the pipe and the effect of the magnetic field on a fully developed velocity profile is studied. ANSYS Fluent® is used for the analysis with periodic boundary conditions, applied at the inlet and outlet to study the fully developed flow of liquid sodium metal. MHD boundary conditions are chosen as electrically insulating boundary conditions. For Pressure-Velocity coupling, the SIMPLE scheme is used. Moreover, momentum, energy, pressure, and magnetic field equations have been discretized with the second-order upwind scheme. A 2D axisymmetric pipe geometry was constructed in the design modular, having a length (L) and diameter (d) of 300 mm and 10 mm, respectively. One radial side of the pipe was set as an inlet and the other as an outlet, and the other two sides are set as wall and axis.

In this study, the temperature is varied from 150 to 450°C and Re is varied from 50 to 400, respectively. Simulations are designed in such a way that temperature is varied from 150 to 450°C with an increment of 75°C at Re 50, 200, 300, and 400. The temperature range is selected based on the temperature changes in different applications of metal flow. Similarly, Re is kept small enough to remain within the laminar regime. An increase in Re from the selected range will start exhibiting small-scale flow disturbances, which will require a reduction in the mesh size. Moreover, a decrease in Re will also increase the computational cost. Ha is varied from 50 to 550 and is found to be one of the key parameters in the MHD flows along with the Re, as increasing Ha has the retarding effect on the fluid field, because of the traverse magnetic field [21]. At Ha = 500, the change in the flow is large enough for the measurement [21].

A mesh-independent study was performed to investigate the effect of mesh density on the solution accuracy and time of calculation with convergence criteria set as root mean square deviation of 10^{-4}. The effect of mesh refinement on maximum flow velocity (U_{max}) is presented in Fig. 4. By increasing the refinement of mesh from 4 to 8 divisions per millimeter (Div mm^{-1}), U_{max} is calculated. Moreover, the biasness factor (which is the ratio of the largest to the smallest edge) of 3 was applied in the region closer to the wall to capture the small changes. When refinement is increased from 4 to 6 Div mm^{-1}, a deviation of 0.142 % was observed in the U_{max}, whereas with a further increase in refinement from 6 to 8 Div mm^{-1}, this deviation is≈0.05 %.

It shows that U_{max} converges on mesh den sity of 6 Div mm^{-1} accurately to four significant figures. It is also observed that a 1 Div mm^{-1} increase in the refinement, doubles the simulation time. Considering the time constraint and accuracy of results, mesh with the refinement of 6 Div mm^{-1} was selected for the study. The mesh obtained with this refinement is shown in Fig. 4.

RESULTS AND DISCUSSION

The effect of variation of magnetic field strength on the developed velocity profile is studied for low Re_m in a range of 10^{-2} to 10^{-6}. With the variation of Re from 50 to 400 and field strength from 0 to 0.4 T, the flow

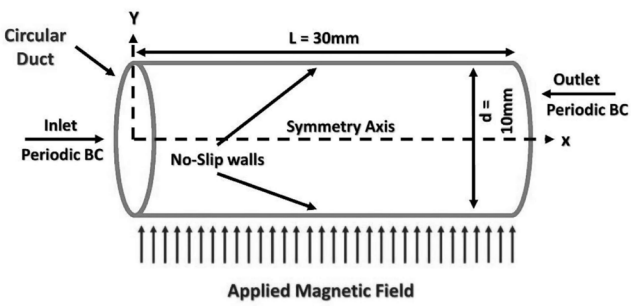

Fig. 3. Schematic diagram of circular duct in a uniform magnetic field.

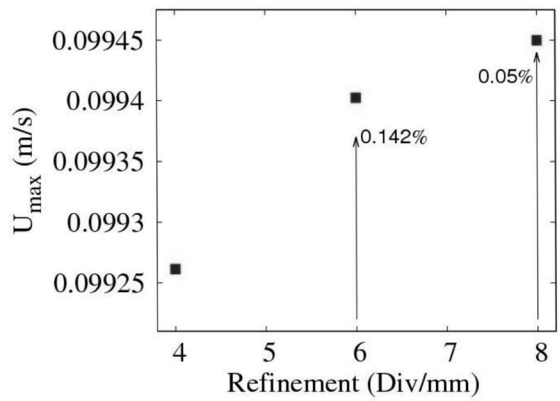

Fig. 4. Mesh independent study (effect of refinement on U_{max}).

dynamics are studied at a temperature range of 150 to 450°C. It is observed that a change in magnetic field strength results in the modification of the inertial velocity profile. Fig. 5 shows the effect of the magnetic field on the velocity profile of liquid sodium at Re = 50 and T = 150°C, where velocity is normalized with the maximum velocity without magnetic field ($U_{o,max}$) and the distance in y direction is normalized by the radius.

At low field strength (0.01 T), the magnetic field acts to flatten the parabolic profile and decreases U_{max}, this is known as the electromagnetic braking effect, and the boundary layer is called the Hartmann boundary layer. This is a typical case when an incompressible fluid flows in a channel and B is applied perpendicular to the wall. Our method successfully captures the Hartmann boundary layer.

Moreover, at field strengths of 0.2 to 0.4 T, an overshoot in velocity is evident near the wall. This overshoot causes the development of an M-shaped velocity profile at higher magnetic field strength, following the study of Holroyd [22] and Swain [23], where the former analysed the flow of liquid metals in rectangular ducts and later worked on MHD flow of Pb-Li through a bend.

Similarly, velocity contours and vectors are also plotted at different field strengths to visualize the M-shaped velocity profile in Fig. 6. The near wall region is zoomed in to have a magnified view of the velocity change. These contours also show that the velocity profile is parabolic at low field strength, which progressively converted to an M-shape with increasing field strength.

This M-shaped profile shown in Fig. 5 (lines representing 0.2 and 0.4 T), has 3 distinct regions; i) Uniform flow in the central region of the pipe at low velocity, ii) a high-velocity region near the wall, and iii) velocity drop along the wall due to no-slip condition. This characteristic M-shape is due to low current density at sidewalls, which lowers the conductivity and the velocity. It also significantly reduces the Lorentz force near the wall in comparison to the mid-region. This asymmetric behaviour of the Lorentz force, which acts in a direction opposite to the flow, increases the velocity near walls and reduces it in the central region.

The overshoot in the velocity is also very important, as it can start local flow disturbances when the local Re is high enough. It is noteworthy that at 0.2 T, the overshoot is 1.1 times the core velocity, and at 0.4 T, it's 1.4 times

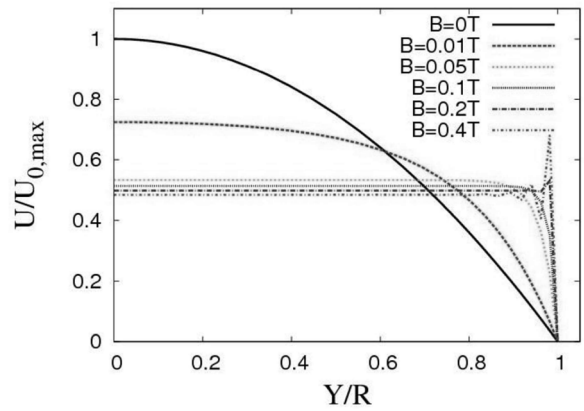

Fig. 5. Velocity Profiles under different magnetic field strengths at Re = 50 and T = 150°C.

the core velocity. This overshoot value is low enough to remain in the laminar region. It is reported that at very high magnetic fields this overshoot can even rise to 3-5 times the core velocity [23].

Fig. 7 shows that for a given temperature, U_{max} first decreases as Lorentz force suppresses the full velocity profile, whereas, with a further increase in the magnetic field, an M-shaped velocity profile is induced, increasing the maximum velocity. This also demonstrates that at a given field strength, maximum velocity decreases with increasing temperature. This decrease is more pronounced at higher B values, whereas less change is evident at small B values. This effect is attributed to a decrease in viscosity, caused by the increase in temperature. It is calculated that for a given field strength, a decrease in U_{max} is 14 % on average with each 75°C drop in temperature for Re = 50.

It is also evident that the change of velocity with field strength is not uniform at a given temperature. For a given temperature, the change in maximum velocity (ΔU_{max}) per unit change in field strength (ΔB) is large at low field strength. Moreover, Fig. 7 also depicts that this change is negligible between 0.05 to 0.2 T. This is the region, where the magnetic field dampens the velocity field, without overshooting near the wall. Similar trends can be seen up to Re 400, as shown in Fig. 7 b - d where it could be seen that the maximum velocity increases significantly with an increase in Re for a given temperature. This increase in U_{max} plays a critical role in the measurements of flow rate, as higher velocity produces higher voltage, after interacting with

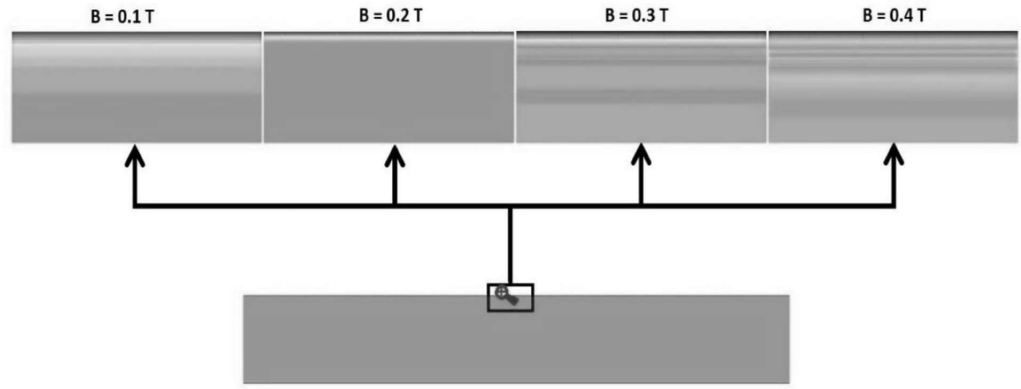

(a) Velocity Contours

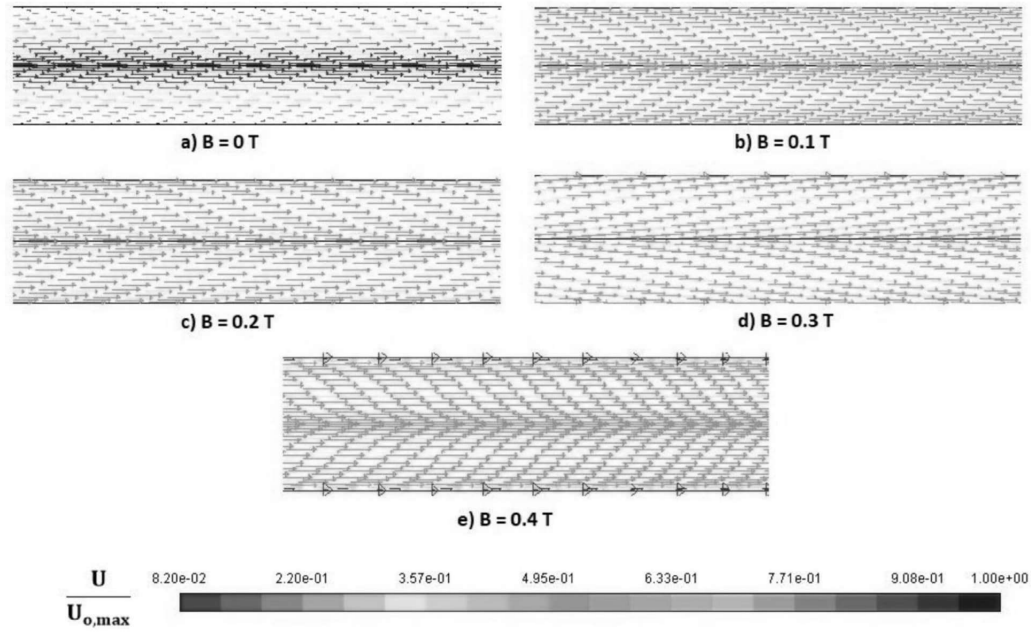

(b) Velocity Vectors

Fig. 6. Normalized velocity contours and vectors at different field strengths, where normalization is done with the maximum velocity at 0 T ($U_{0,\,max}$).

the Lorentz force.

For the sake of calibration of the flow meter, one needs to know the variation of Lorentz force and voltage at different temperatures and Re. This calibration data is presented in Fig. 8 and Fig. 9. These figures show the trend of the voltage signal and the Lorentz force against the Re at different temperatures and field strengths. These figures show that at a given B, voltage and Lorentz force decreases with increasing temperature. Moreover, both voltage and Lorentz force increases with increasing B at a given temperature. Quantitatively, per unit change in voltage is 0.00029 mV at 150°C and it decreases onward to 0.00014 mV at 450°C at B = 0.4 T. The sensitivity of the instrument is thus dependent on temperature.

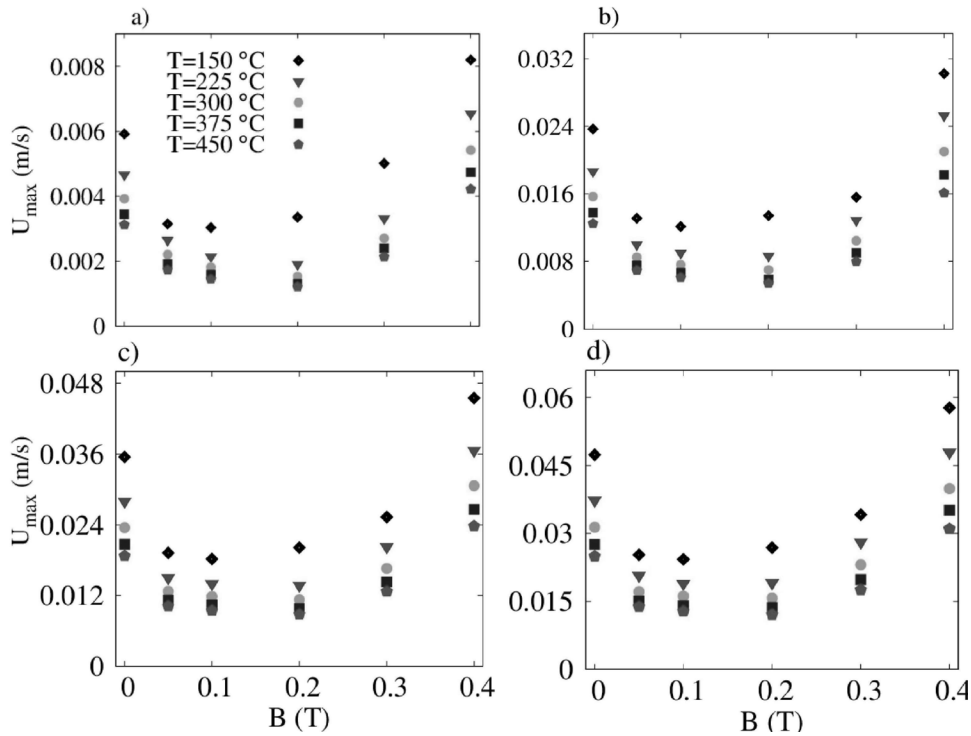

Fig. 7. Change in U_{max} with field strengths for different temperatures at (a) Re = 50, (b) Re = 200, (c) Re = 300, and (d) Re = 400.

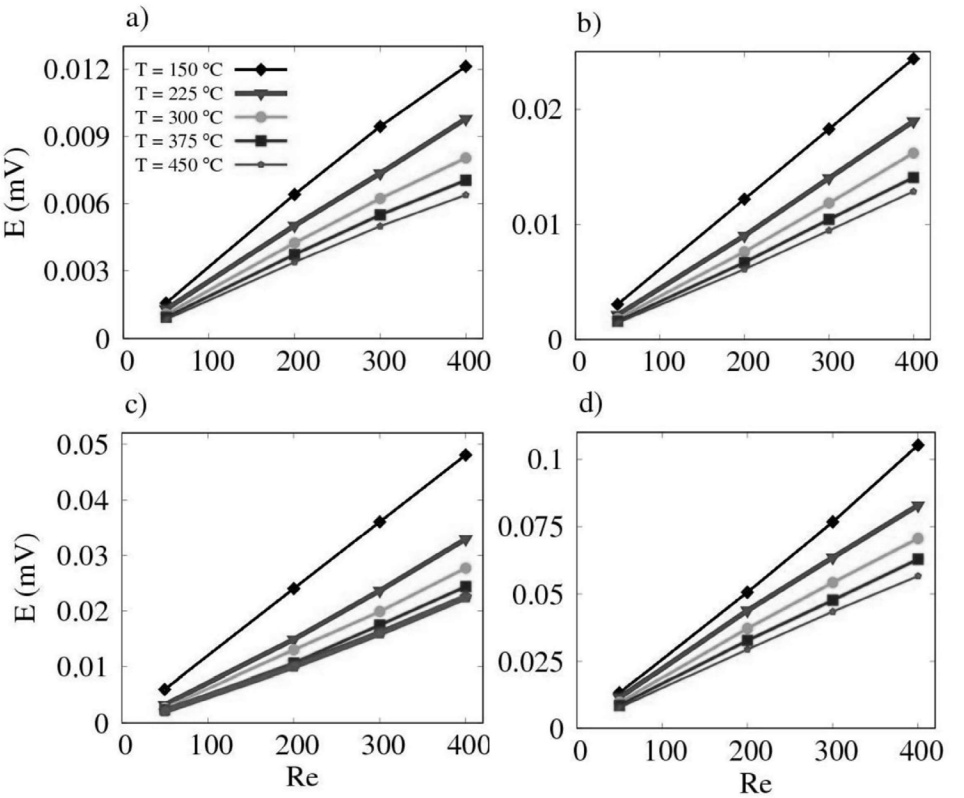

Fig. 8. Calibration data of voltage against Re for different temperatures at (a) B = 0.05 T, (b) B = 0.1 T, (c) B = 0.2 T, (d) B = 0.4 T.

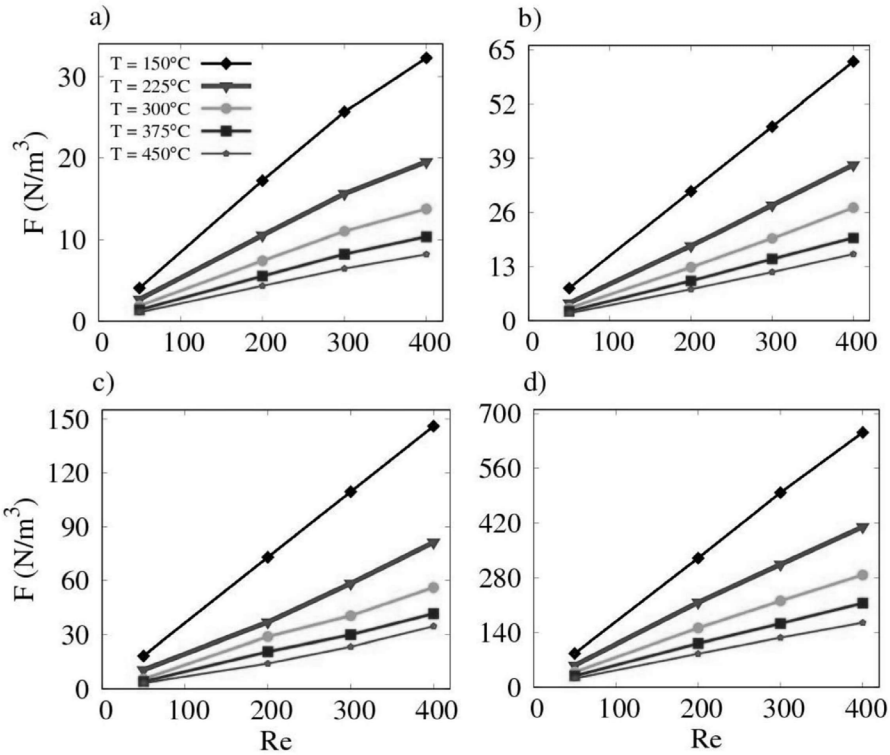

Fig. 9. Calibration data of Lorentz force against Re for different temperatures at (a) B = 0.05 T, (b) B = 0.1 T, (c) B = 0.2 T, (d) B = 0.4 T.

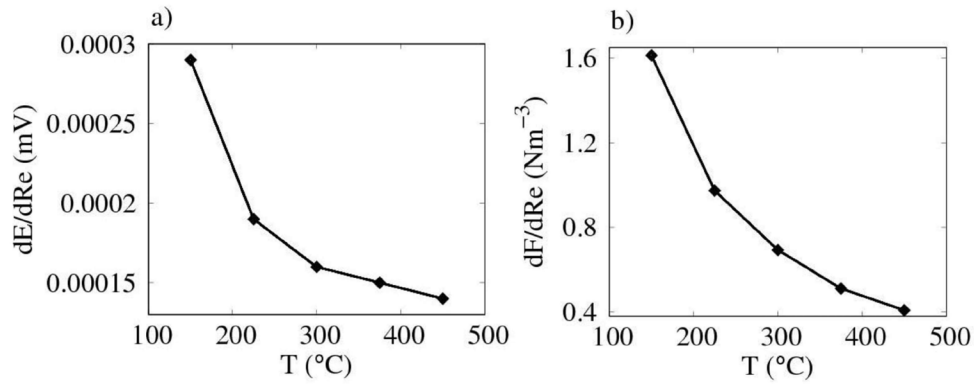

Fig. 10. Sensitivity of voltage and Lorentz force per unit change in Re against temperature at B = 0.4 T.

The sensitivity of voltage data at different temperatures is presented in Fig. 10 at B = 0.4 T. It shows that at higher temperatures, the sensitivity of voltage signals per unit change in Re is small. This decrease in the sensitivity at higher temperatures is due to reduced magnitudes of induced currents, caused by the decrease in electrical conductivity. Conductivity decreases by approximately 15 % for each 75°C change in temperature. As the current density is directly proportional to conductivity ($J \propto \sigma$), the current density and voltage also decreases with the increase in temperature. Similarly, the behaviour of Lorentz force with Re is also dependent on system temperature. The sensitivity for Lorentz force with

temperature is also presented in Fig. 10. It shows that at higher temperatures, Lorentz force is less sensitive towards the per unit change in Re. For 150°C per unit change in force is 1.6 N m^{-3} and this decreases to 0.4 N m^{-3} at 450°C. Similar calculations can also be done at other field strengths. This trend is directly related to the trend of current density. The higher the induced current density in the region, the greater its interaction with the applied magnetic field to produce the reaction force i.e., Lorentz force ($F \propto J$). This table clearly shows the range of operation of flow meters. Since these meters are very sensitive to the temperature range, hence, it should be operated in low temperature regimes i.e., at a temperature ≤ 300°C.

CONCLUSIONS

Numerical simulations are performed to investigate the application of magnetic flow meters for the liquid metal flow measurements. The commercial CFD package ANSYS Fluent® embedded with an MHD module is used to investigate the sensitivity of these magnetic flow meters for liquid sodium. It is observed that the inertial parabolic velocity profile changes with the change in the magnetic field. At low field strengths, the magnetic field acts to dampen the overall velocity profile and makes it more uniform until a reversal in behaviour occurs. With further increase in the magnetic field i.e., B ≥ 0.2 T, an overshoot is observed near the wall, along with the dampening of the velocity profile. These velocity overshoots develop into M-shaped profiles at very high field strengths. Due to this modification, the maximum velocity in the pipe shows a decreasing-increasing trend with the increase of field strength. This behaviour is observed at higher magnetic field strengths, because of the low viscosity of the fluid at high temperatures, which flattens the overall velocity profile. At high Re, the effect of the magnetic field on flow is amplified, as Lorentz's force is directly proportional to the inertial flow velocity. Similarly, it is observed that the sensitivity of voltage and Lorentz force with the change of Re is directly related to field strength and temperatures. It is concluded that the best results for the magnetic flow meters can be achieved at low temperature, high Re, and high magnetic field strengths. At these conditions, maximum velocity and per unit change in voltage and Lorentz force are large, which makes the measurement feasible.

Acknowledgment

Thanks to the Department of Chemical Engineering, PIEAS, for its computational facilities which led to the completion of the project.

Authors' contribution: *F.S.: Execution of simulation, Data analysis, Writing - manuscript; M.N.: Conceptualization, Discussions, M.U.: Data analysis, Writing - manuscript; S.H.: Conceptualization, Proof reading; A.H.: Conceptualization, Proof reading, Supervision.*

REFERENCES

1. J. L. Neuringer, R. E. Rosensweig, Ferrohydrodynamics, Phys. Fluids, 7, 1964, 1927-1937.
2. O. Prakash, S.P. Singh, D. Kumar, Y. K. Dwivedi, A study of effects of heat source on MHD blood flow through bifurcated arteries, AIP Adv., 1, 2011, 42128.
3. C. Heinicke, S. Tympel, G. Pulugundla, I. Rahneberg, T. Boeck, A. Thess, Interaction of a small permanent magnet with a liquid metal duct flow, J. Appl. Phys., 112, 2012, 761-788.
4. A. Serizawa, T. Ida, O. Takahashi, I. Michiyoshi, MHD effect on NaK-nitrogen two-phase flow and heat transfer in a vertical round tube, Int. J. Multiph. Flow, 16, 1990, 761-788.
5. A. Khalid, I. Khan, A. Khan, S. Shafie, I. Tlili, Case study of MHD blood flow in a porous medium with CNTS and thermal analysis, Case Stud. Therm. Eng., 12, 2018, 374-380.
6. M. Sheikholeslami, R. Ellahi, Three-dimensional mesoscopic simulation of magnetic field effect on natural convection of nanofluid, Int. J. Heat Mass Transf., 89, 2015, 799-808.
7. S. Cuevas, B.F. Picologlou, J.S. Walker, G. Talmage, Liquid-metal MHD flow in rectangular ducts with thin conducting or insulating walls: Laminar and turbulent solutions, Int. J. Eng. Sci., 35, 1997, 485-503.
8. K. Natesan, K. Velusamy, Coupled system dynamics and computational fluid dynamics simulation of plant transients in sodium cooled fast reactors, Nucl. Eng. Des., 342, 2019, 157-169.
9. Y. L. Liu, D. Chen, P. Shang, D. C. Yin, A review of

magnet systems for targeted drug delivery, J. Control. Release, 302, 2019, 90-104.

10. Ch. Alexiou, A. Schmidt, R. Klein, P. Hulin, Ch. Bergemann, W. Arnold, Magnetic drug targeting: biodistribution and dependency on magnetic field strength, J. Magn. Magn. Mater., 252, 2002, 363-366.
11. M. Ghalambaz, M. Sabour, S. Sazgara, I. Pop, R. Trâmbiţaş, Insight into the dynamics of ferrohydrodynamic (FHD) and magnetohydrodynamic (MHD) nanofluids inside a hexagonal cavity in the presence of a non-uniform magnetic field, J. Magn. Magn. Mater., 497, 2020, 166024.
12. H.R. Kim, Y.B. Lee, MHD stability analysis of a liquid sodium flow at the annular gap of an EM pump, Ann. Nucl. Energy, 43, 2012, 8-12.
13. U. Jeong, T.J. Kim, Y.H. Kim, H.H. Son, Department of Nuclear Engineering, Hanyang University, 222 Wangsimni-ro, Seongdong-gu, Seoul133-791, Republic of Korea, Gwang Hyeok Seo &Sung Joong Kim, Numerical evaluation of SmCo permanent magnet flowmeter measuring sodium flow in a low flow rate regime using FLUENT/MHD module, J. Nucl. Sci. Technol., 53, 2016, 173-183.
14. K.K. Rajan, V. Sharma, G. Vijayakumar, T. Jayakumar, Development of side wall type permanent magnet flowmeter for sodium flow measurement in large pipes of SFRs, Flow Meas. Instrum., 42, 2015, 69-77.
15. B.K. Nashine, P. Sharma, G. Vijayakumar, V. Sharma, S. Narmadha, S. Chandramouli, V. Prakash, P. Selvaraj, Development of Electromagnetic Devices for Sodium Cooled Fast Reactor Application, Fast Reactors and Related Fuel Cycles, 2017, 1-10.
16. X. Wang, Y. Kolesnikov, A. Thess, Numerical calibration of a Lorentz force flowmeter, Meas. Sci. Technol., 23, 2012, 045005.
17. V. Sharma, S. Narmadha, S.K. Dash, R. Veerasamy, B.K. Nashine, K.K. Rajan, P. Kalyanasundaram, Probe Type Permanent Magnet Flowmeter, COMSOL Conference India, 2010, 3-6.
18. M. Tarabad, R. C. Baker, Integrating electromagnetic flowmeter for high magnetic Reynolds numbers, J. Phys. D. Appl. Phys., 15, 1982, 739.
19. ANSYS, ANSYS Fluent - CFD Software, 2016, 3-6.
20. A. Altintas, I. Ozkol, Magnetohydrodynamic Flow of Liquid-Metal in Circular Pipes for Externally Heated and Non-Heated Cases, J. Appl. Fluid Mech., 8, 2015, 507-514.
21. J. Srinivas, J.V. Ramana Murthy, Thermodynamic analysis for the MHD flow of two immiscible micropolar fluids between two parallel plates, Front. Heat Mass Transf., 6, 2015, 601.
22. R.J. Holroyd, An experimental study of the effects of wall conductivity, non-uniform magnetic fields and variable-area ducts on liquid metal flows at high Hartmann number. Part 1. Ducts with non-conducting walls, J. Fluid Mech., 93, 1979, 609-630.
23. P.K. Swain, P. Satyamurthy, R. Bhattacharyay, A. Patel, A. Shishko, E. Platacis, A. Ziks, S. Ivanov, A.V. Despande, 3D MHD lead–lithium liquid metal flow analysis and experiments in a Test-Section of multiple rectangular bends at moderate to high Hartmann numbers, Fusion Eng. Des., 88, 2013, 2848-2859.